Konrad-Zuse-Zentrum
für Informationstechnik Berlin

Takustraße 7
D-14195 Berlin-Dahlem
Germany

WILHELM HUISINGA[1], LORENZO PESCE[2 3], RONNIE KOSLOFF[4 3], AND PETER SAALFRANK[2 5]

Faber and Newton Polynomial Integrators for Open-System Density Matrix Propagation

[1]Konrad-Zuse-Zentrum für Informationstechnik Berlin, Takustraße 7, D-14195 Berlin, Germany

[2]Institut für Physikalische und Theoretische Chemie, Freie Universität Berlin, Takustraße 3, D-14195 Berlin, Germany

[3]Present address: Department of Chemistry, Northwestern University, 2145 Sheridan Road, Evanston, IL 60208, USA

[4]Department of Physical Chemistry, Hebrew University Jerusalem, Jerusalem 91904, Israel

[5]Chemistry Department, University College London, 20 Gordon Street, London WC1H 0AJ, U.K.

Preprint SC 98-29 (November 1998)

Abstract

Two polynomial expansions of the time-evolution superoperator to directly integrate Markovian Liouville-von Neumann (LvN) equations for quantum open systems, namely the Newton interpolation and the Faber approximation, are presented and critically compared. Details on the numerical implementation including error control, and on the performance of either method are given. In a first physical application, a damped harmonic oscillator is considered. Then, the Faber approximation is applied to compute a condensed phase absorption spectrum, for which a semi–analytical expression is derived. Finally, even more general applications are discussed. In all applications considered here it is found that both the Newton and Faber integrators are fast, general, stable, and accurate.

1 Introduction

The quantum dynamical, often time–dependent, microscopic description of molecular systems has seen a big leap forward in recent years [1]. In particular the treatment of complex molecules or molecules in an environment (in solution, in a matrix, in a solid, or at a surface) is in the focus of actual theoretical research [1].

The quantum dynamics of "open" systems, *e.g.*, those exchanging energy and phase with their surroundings, are frequently treated within open system density matrix theory [2]. In cases where the characteristic timescales of motion of the environmental modes are fast the Markov approximation can be made, which neglects memory effects [2]. The problem then comes down to the solution of a Markovian, open–system Liouville-von Neumann equation of the form ($\hbar := 1$):

$$\dot{\hat{\rho}}(t) = \mathcal{L}\hat{\rho}(t) = -i[\hat{H}_s, \hat{\rho}(t)] + \mathcal{L}_D\hat{\rho}(t) \quad . \tag{1}$$

Here, $\mathcal{L}$ is the total, and $\mathcal{L}_D$ the dissipative Liouvillian. These are linear functions of the actual, "reduced" density operator $\hat{\rho}$, the latter depending on the typically few molecular ("system") degrees of freedom only. $\hat{H}_s$ is the corresponding system Hamiltonian, which is to be understood as an effective Hamiltonian because it may include the static (averaged) distortion of the system dynamics due to the "reservoir", or "bath". Energy and phase exchange between the system and the bath ("relaxation" and "dephasing") are hidden in the dissipative Liouvillian $\mathcal{L}_D$, the proper choice of which ist still a matter of scientific dispute [3]. It is even unclear whether under the Markov approximation such a "proper" choice (*i.e.*, one which does not violate basic physical principles such as equipartitioning or non–occurrence of negative probabilities) is possible at all [3]. The most prominent examples of how to choose $\mathcal{L}_D$ have been given by Redfield ("Redfield" theory) [4], and by Lindblad and others ("dynamical semigroup approach") [5, 6]. Existing alternative choices [7] for $\mathcal{L}_D$ can be shown to be often closely related to existing schemes such as Redfield theory [3].

Once Equ.(1) is solved, *i.e.*, $\hat{\rho}(t)$ known, the relevant observables are readily computed from a quantum mechanical trace,

$$\langle \hat{A} \rangle (t) = \mathrm{tr}\{\hat{A}\hat{\rho(t)}\} \quad .$$

Except for special examples, an analytical solution of Equ.(1) is not available and one has to resort to a numerical treatment. The latter requires (i) a particular representation of the operators, and (ii) a time integration scheme. Assuming that a certain representation was selected (*e.g.*, discrete spatial grids [8, 9, 23], zeroth order or other state representation [11, 12, 13], or mixed ones [14, 15]), Equ.(1) can be written as a matrix differential equation

$$\dot{\boldsymbol{\rho}}(t) = \boldsymbol{\mathcal{L}}\boldsymbol{\rho}(t) \quad , \tag{2}$$

with the initial condition $\boldsymbol{\rho}(0) = \boldsymbol{\rho}_0$. Here, $\boldsymbol{\mathcal{L}}$ is a $D \times D$ matrix representation of the Liouvillian and $\boldsymbol{\rho}_0$ is a "vector" of size $D = N \times N$, where N is the size of the Hilbert space of the system. Analytically, the solution of (2) for a time $\tau \geq 0$ is

$$\boldsymbol{\rho}(\tau) = \exp(\tau\boldsymbol{\mathcal{L}})\boldsymbol{\rho}_0 \quad . \tag{3}$$

Equ.(3) will be referred to as a "direct", or matrix solution of the LvN equation (1).

The direct solution is to be contrasted with indirect ones, for which (many) stochastically sampled or variationally determined, (coupled) wave packets are employed. Examples of these wave packet based methods are the Monte Carlo Wave Packet (MCWP) [17, 18, 19, 20, 21, 10], the Quantum State Diffusion (QSD) [22, 10, 23], and the Variational Wave Packet (VWP) methods [24, 25], respectively. Both classes of solution techniques (direct or indirect) require different computational resources (memory occupation and computation time), differ in their accuracy (*e.g.*, statistical convergence *vs.* numerically "exact"), and are not equally generally applicable (*e.g.*, restricted to Lindblad forms of dissipation). Whether or not one or the other approach offers computational advantages is, therefore, quite system- and problem-dependent [21]. The direct methods serve, at a minimum, as accurate and general benchmarks.

In the practice of direct methods the exponential of a large matrix has to be approximated. Various approaches have been proposed to do so. Besides "brute–force" direct diagonalization of the Liouvillian [26] and general–purpose Runge–Kutta integration [23, 11], there are more sophisticated schemes such as various split–operator techniques [8, 10, 27], Krylov methods [12], and polynomial expansions [28, 29, 30, 14, 15, 16].

The polynomial expansions, which will be the focus of the present paper, have the distinct advantage of being (arbitrarily) accurate but still efficient. In the following, two specific examples of how to approximate the time-evolution superoperator $\exp(\tau\boldsymbol{\mathcal{L}})$ in Equ.(3) will be considered in some detail. The first one is a Newton interpolation, which has been used earlier for density matrix propagation [28, 29, 30, 14, 15, 16]. The second is an approximation of $\exp(\tau\boldsymbol{\mathcal{L}})$ based on Faber polynomials – these haven't been used so far to propagate density matrices in time, but proved useful for approximating the Green operator for time–independent scattering calculations or to compute a propagator $e^{-i\tilde{\hat{H}}t}$ with non–Hermitean Hamiltonian $\tilde{\hat{H}}$ [31].

We will provide a unified mathematical background for both types of polynomial expansions (Sec.2), and a critical evaluation of numerical aspects of their implementation, stability, and performance (Sec.3). In Sec.4, examples for the application of the Newton and Faber methods to physical problems will be given. In Sec.4.1 both methods will be applied to a damped harmonic oscillator. In Sec.4.2, a semi–analytical series expansion based on Faber polynomials for continuous wave (cw), condensed phase absorption spectra will be derived. We apply the new series to the dissipative infrared (IR) absorption spectrum of benzoic acid dimers in a crystalline environment. In Sec.4.3 it will be argued that the Faber and Newton techniques can also be efficiently applied to explicitly time–dependent problems, and are general enough to treat any kind of (Markovian) dissipation. A final section 5 concludes our work.

2 Newton and Faber polynomial integrators

2.1 General aspects

If we choose a polynomial approximation for the time evolution superoperator, we are interested in a polynomial $P_n^\tau(\boldsymbol{\mathcal{L}})\boldsymbol{\rho}_0$ which minimizes among all polynomials of degree $\leq n$ the *local error*

$$\epsilon_{\rm loc}(n) = \|\exp(\tau\boldsymbol{\mathcal{L}})\boldsymbol{\rho}_0 - P_n^\tau(\boldsymbol{\mathcal{L}})\boldsymbol{\rho}_0\|. \tag{4}$$

To further proceed we first note that the eigenvalue spectrum of the Liouvillian is complex. The eigenvalues are distributed symmetrically with respect to the real axis, because their imaginary part derives from the Hamiltonian Liouvillian $\mathcal{L}_H := -i[\hat{H}_s, \bullet]$ in Equ.(1). This term corresponds to all the possible differences between the eigenvalues of $\hat{H}_s$, that is the imaginary frequencies $i\omega_{ij} = i\,(E_i - E_j)$. Further, the eigenvalues are usually (*i.e.*, for energy–withdrawing processes) located in the left half of the complex plane, indicating negative real parts due to the dissipative Liouvillian $\mathcal{L}_D$.

The application of functional calculus of analytic functions [32] gives an insightful framework to approximate a function of a Liouvillian with complex spectrum. Let $\Gamma \subset \mathbb{C}$ be any closed (Jordan) curve that does not intersect itself (*e.g.*, the boundary of a rectangle or an ellipse) enclosing the spectrum of $\boldsymbol{\mathcal{L}}$; then

$$
\begin{aligned}
\epsilon_{\mathrm{loc}}(n) &= \|\exp(\tau\boldsymbol{\mathcal{L}})\boldsymbol{\rho}_0 - P_n^\tau(\boldsymbol{\mathcal{L}})\boldsymbol{\rho}_0\| \\
&= \|\frac{1}{2\pi i}\int\limits_\Gamma \{\exp(\tau z) - P_n^\tau(z)\}(z\mathbf{I} - \boldsymbol{\mathcal{L}})^{-1}\boldsymbol{\rho}_0\,dz\| \\
&\leq \min_\Gamma\left\{C_\Gamma \max_{z\in\Gamma}|\exp(\tau z) - P_n^\tau(z)|\right\}
\end{aligned}
$$

for a constant $C_\Gamma > 0$, depending on $\boldsymbol{\mathcal{L}}$ and Γ, but independent of n. From the above inequality, we see that the local error is related to the problem of approximating a scalar analytic function, *i.e.*, finding among all polynomials P_n^τ at most of degree n one that minimizes for fixed Γ

$$
\max_{z\in\Gamma}|\exp(\tau z) - P_n^\tau(z)| \quad . \tag{5}
$$

Following the maximum principle [33], one can substitute in (5) Γ by the domain $G = G(\Gamma)$ defined as the set of all points enclosed by Γ. The exact solution of the min–max problem requires the calculation of the spectrum of $\boldsymbol{\mathcal{L}}$, equivalent to diagonalize it. This is precisely what we want to avoid, since direct diagonalization of $\boldsymbol{\mathcal{L}}$ is in general inefficient. Therefore, it is a common practice to fix a curve Γ or respectively a domain G and consider the scalar valued approximation problem (5). The choice of the domain G is important for numerical aspects as we are going to see below.

There is a rich literature about the approximation problem (5) both in complex analysis [34, 35, 36] and in theoretical chemistry [1, 31] to cite a few. These different methods can be considered as special realizations of polynomial approximations. In the next subsection, the notion of conformal mapping associated with a domain is introduced to be used in the definition of the "quasi–optimal" polynomial approximation on a domain that includes the eigenvalues of the matrix $\boldsymbol{\mathcal{L}}$.

2.2 Conformal mapping

For a given domain G, it is advantageous to consider separately its geometry from its size. The shape of G determines the form of the polynomial approximation P_n^τ, while the size influences its numerical stability.

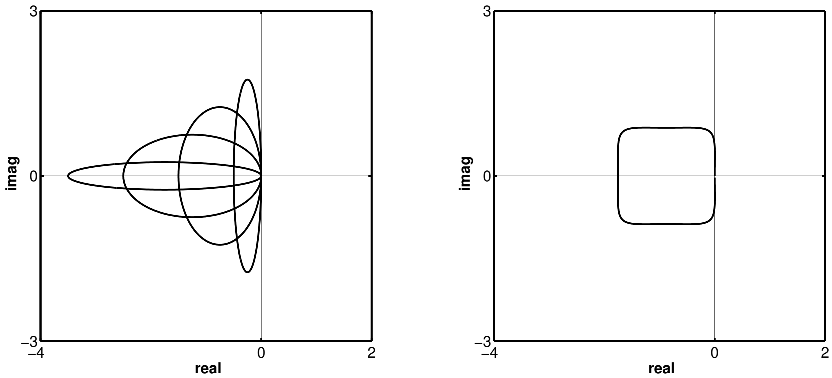

Figure 1: Elliptical and rectangle–like *scaled* domains as in the examples (7) and (8). The parameters are $m = -0.25, -0.75, \ldots, -1.75$ and $d = -(m+1)$ (from the left to the right ellipse) and $m = -0.875$ for the "rectangle".

Let G be a bounded, closed continuum in the complex plane, such that the complement of G is simply connected in the extended plane and contains the point at ∞, *e.g.*, a rectangle or an ellipse. By the Riemann mapping theorem [33], there exists a conformal mapping ψ which maps the complement of a closed disc with center at the origin and radius ρ onto the complement of G, satisfying the normalization condition $\lim_{|w|\to\infty} \psi(w)/w = 1$. Then, its Laurent expansion at ∞ is given by

$$\psi(w) = w + \gamma_0 + \gamma_1 w^{-1} + \gamma_2 w^{-2} + \ldots \qquad (6)$$

with coefficients $\gamma_i \in \mathbb{C}$. The *logarithmic capacity* of G is defined as the radius ρ of the above disc. We call a domain *scaled*, if $\rho = 1$. Two examples may illustrate this:

1. For the herein suggested polynomial integrator, the conformal mapping

$$\psi(w) = w + m + d/w \qquad (7)$$

with parameters $m, d \in \mathbb{C}$ is of central importance. The left picture of Fig. 1 shows that for a given logarithmic capacity ρ, $\psi(w)$ describes a family of ellipses with center at m and minor and major axis $a = (\rho - d/\rho)$ and $b = (\rho + d/\rho)$, respectively.

2. The mapping

$$\psi(w) = w + m - 1/(2w)^3, \qquad m \in \mathbb{C}, \tag{8}$$

specifies a family of "smoothed rectangles", centered at m (see right panel of Fig. 1).

2.3 The Faber approximation

In this section a brief introduction to Faber polynomials is provided. It is interesting to notice that the well known Chebychev polynomials are a special family of Faber polynomials constructed to approximate continuous functions of real variables. When functions of matrices have to be computed, the Chebychev approximation is consequently suited to matrices with real or purely imaginary eigenvalues, like the Hamiltonian, while Faber polynomials are generally appropriate when the eigenvalues are defined in the complex plane.

The family of *Faber polynomials* $\{F_k\}_{k\in\mathbb{N}}$ associated with a conformal mapping ψ is defined via the recursion relation

$$F_{k+1}(z) = z \cdot F_k(z) - \sum_{j=0}^{k} \gamma_j \cdot F_{k-j}(z) - k \cdot \gamma_k \tag{9}$$

for $k \geq 1$ and $F_0(z) \equiv 1$ [37, 38, 31]. The corresponding relations for matrix operations are obtained substituting z by $\boldsymbol{\mathcal{L}}$ and multiplying the equations by $\boldsymbol{\rho}_0$, as is exemplified in Equ.(11) below. The recursion relation is stable, if z or the spectrum of $\boldsymbol{\mathcal{L}}$ respectively are contained in the *scaled* domain [39]. It can be seen from (9) that Faber polynomials, defined by their recursion relation, depend upon the coefficients γ_j of the conformal mapping ψ and thus on the shape of G independently of the size of the domain G [there is no ρ in Equ. (9)].

From a numerical point of view, *e.g.*, for memory occupation, we are interested in the families of Faber polynomials which allow short–term recursions. Thus, we are interested in domains G whose associated conformal mappings have only a few non–zero terms in their Laurent expansion at ∞ [see (6)]. Among them, we have been working mainly with the family of Faber polynomials corresponding to the conformal mapping $\psi(w) = w + m + d/w$ [see example (1) above]. The parameters m and d depend upon the relative strength of the Hamiltonian and dissipative dynamics of the physical problem studied.

For our conformal mapping (7), the associated Faber polynomialis are defined by the three term recursion

$$F_{k+1}(z) \quad = \quad (z-m)F_k(z) - d \cdot F_{k-1}(z), \qquad k > 1 \tag{10}$$

with initial values $F_0(z) \equiv 1$, $F_1(z) = z - m$ and $F_2(z) = (z-m)^2 - 2d$. The matrix equivalents of these relations are

$$F_{k+1}(\boldsymbol{\mathcal{L}})\boldsymbol{\rho}_0 = (\boldsymbol{\mathcal{L}} - m\mathbf{I})F_k(\boldsymbol{\mathcal{L}})\boldsymbol{\rho}_0 - d \cdot F_{k-1}(\boldsymbol{\mathcal{L}})\boldsymbol{\rho}_0, \qquad k > 1 \tag{11}$$

with initial values $F_0(\boldsymbol{\mathcal{L}})\boldsymbol{\rho}_0 \equiv \boldsymbol{\rho}_0$, $F_1(\boldsymbol{\mathcal{L}})\boldsymbol{\rho}_0 = (\boldsymbol{\mathcal{L}} - m\mathbf{I})\,\boldsymbol{\rho}_0$ and $F_2(\boldsymbol{\mathcal{L}})\boldsymbol{\rho}_0 = (\boldsymbol{\mathcal{L}} - m\mathbf{I})\,F_1(\boldsymbol{\mathcal{L}})\boldsymbol{\rho}_0 - 2d \cdot \boldsymbol{\rho}_0$. Setting the parameters m to 0 and d to $1/4$, the associated Faber polynomials F_k are equal to the normalized Chebychev polynomials T_k via $F_k(z) = 2^{1-k}T_k$, for $k \geq 1$, while $F_0 = T_0$.

Any function that is analytic inside G can be expanded in terms of the Faber polynomials associated with ψ [37, 40, 38]. In application to $\exp(\tau z)$, this yields:

$$\exp(\tau z) = \sum_{k=0}^{\infty} \underbrace{\frac{1}{2\pi i} \int_{|w|=1} \frac{\exp(\tau\psi(w))}{w^{k+1}}\, dw}_{c_k(\tau)} \; F_k(z) \tag{12}$$

for all $z \in G$. Equ.(12) is exact. Now we define the *Faber approximation* of order n to be the truncated series

$$P_n^\tau(z) = \sum_{k=0}^{n} c_k(\tau) F_k(z)$$

with expansion coefficients as defined above. Substituting $F_k(z)$ by $F_k(\boldsymbol{\mathcal{L}})\boldsymbol{\rho}_0$, one gets the "matrix valued version" $P_n^\tau(\boldsymbol{\mathcal{L}})\boldsymbol{\rho}_0$

$$\boldsymbol{\rho}(\tau) = \exp(\tau\boldsymbol{\mathcal{L}})\boldsymbol{\rho}_0 \approx P_n^\tau(\boldsymbol{\mathcal{L}})\boldsymbol{\rho}_0 = \sum_{k=0}^{n} c_k(\tau) F_k(\boldsymbol{\mathcal{L}})\boldsymbol{\rho}_0 \quad . \tag{13}$$

For our conformal mapping $\psi(w) = w + m + d/w$, the coefficients can be solved analytically

$$\begin{aligned} c_k(\tau) \quad &= \quad \frac{1}{2\pi i} \int_{|w|=1} \frac{\exp\left(\tau(w + m + d/w)\right)}{w^{k+1}}\, dw \\ &= \quad (-i/\sqrt{-d})^k \exp(\tau m) J_k(2\tau\sqrt{-d}), \end{aligned} \tag{14}$$

where we used the identity $\exp\left(x(t + 1/t)/2\right) = \sum_k (t/i)^k J_k(ix)$ [41]. Here, J_k is a Bessel function of the first kind. For $d = 0$ the conformal mapping ψ is a simple translation. Thus, Equ. (12) is simply the power series expansion at point m. From now on, the term "Faber approximation" is always meant with respect to the conformal mapping (7).

2.4 The Newton interpolation at Lejá points

Another way to approximate functions of matrices with polynomials is suggested by the theory of the interpolation of analytic functions. The complex Newton interpolation based on Lejá points is an efficient implementation of this idea, and was introduced in density matrix calculations by Kosloff, Tal-Ezer and Berman [28, 16]. The method is shortly outlined in the following.

Let G be a domain as defined in Section 2.2. A sequence $(z_m)_{m\in\mathbb{N}}$ of points on the boundary of G, *i.e.*, $(z_m)_{m\in\mathbb{N}} \subset \Gamma$, is called a *Lejá point sequence* [36], if $|z_1| = \max_{z\in G}|z|$ and

$$\prod_{k=1}^{m} |z_{m+1} - z_k| = \max_{z\in G} \prod_{k=1}^{m} |z - z_k|$$

for $m > 1$[6]. In numerical applications, one substitutes the maximum of all $z \in \Gamma$ by the maximum of all $z \in \Gamma_L$, where $\Gamma_L = \{\tilde{z}_1, \tilde{z}_2, \tilde{z}_3, ...\tilde{z}_L\}$ is a set of uniformly distributed points on the boundary of G with $L \gg n =$ (estimated) degree of P_n^τ. We call a Lejá point sequence *scaled* if the points lie on the boundary of a *scaled* domain.

A sequence of Lejá points defines the associated Newton polynomials $\{\omega_k(z)\}_{k\in\mathbb{N}}$ by the two term recursion

$$\omega_{k+1}(z) \quad = \quad (z - z_{k+1})\,\omega_k(z) \tag{15}$$

for $k \geq 0$ and $\omega_0(z) \equiv 1$. The relations used for functions of matrices are defined by

$$\omega_{k+1}(\boldsymbol{\mathcal{L}})\boldsymbol{\rho}_0 = (\boldsymbol{\mathcal{L}} - z_{k+1}\mathbf{I})\,\omega_k(\boldsymbol{\mathcal{L}})\boldsymbol{\rho}_0 \tag{16}$$

with starting term $\omega_0(\boldsymbol{\mathcal{L}})\boldsymbol{\rho}_0 \equiv \boldsymbol{\rho}_0$. The recursion relation is stable if the Lejá points are *scaled* and z (or the spectrum of $\boldsymbol{\mathcal{L}}$ respectively) is contained in the *scaled* domain [36].

The Newton polynomials are related to the logarithmic capacity ρ of G by $\sqrt[m+1]{|\omega_m(z_{m+1})|} \longrightarrow \rho$ for $m \to \infty$ thus

$$|\omega_m(z_{m+1})| \approx \rho^{m+1} \tag{17}$$

for "large" m. This shows why scaled Lejá points are necessary to avoid overflows (underflows) [42, 36].

[6]For the numerical purposes, z_1 can be any point $\in \Gamma$.

The coefficients entering a Newton series are the so called divided differences. For a function f on G, the divided differences can be defined recursively[7] :

$$[z_k, \ldots, z_l]f = \frac{[z_{k+1}, \ldots, z_l]f - [z_k, \ldots, z_{l-1}]f}{z_l - z_k} \tag{18}$$

for $1 \leq k < l$ and initial values $[z_k]f = f(z_k)$.

Let ψ be the conformal mapping associated with a domain G. Then, any function that is analytic inside G can be expanded in terms of the Newton polynomials associated with the Lejá points $(z_m)_{m\in\mathbb{N}}$ [37, 40, 36]. The application to $f(z) = \exp(\tau z)$ yields

$$\exp(\tau z) = \sum_{k=0}^{\infty} [z_1, \ldots, z_{k+1}]\mathrm{exp}\ \omega_k(z)$$

for all $z \in G$. Now we define the *Newton interpolation* of order n as the truncated series

$$\exp(\tau z) \approx P_n^\tau(z) \ = \sum_{k=0}^{n} [z_1, \ldots, z_{k+1}]\mathrm{exp}\ \omega_k(z) \quad .$$

Substituting $\omega_k(z)$ by $\omega_k(\boldsymbol{\mathcal{L}})\boldsymbol{\rho}_0$ one gets the "matrix valued version" $P_n^\tau(\boldsymbol{\mathcal{L}})\boldsymbol{\rho}_0$ that is formally equivalent to relation (13).

3 Numerical aspects

Analytically, the Faber approximation and the Newton interpolation are very similar [39]. It has to be checked whether this holds true also numerically. Before starting, we have to decide how to choose the domain that includes the eigenvalues of $\boldsymbol{\mathcal{L}}$. This step is very similar for the two algorithms.

3.1 On scaling and domain

The effects of the choice of the domain on the numerical stability and efficiency are of general nature, so any system can be used to exemplify them. For this purpose we have chosen an abstract model dissipative system. Here $\boldsymbol{\mathcal{L}}$ corresponds simply to a diagonal matrix with complex eigenvalues, shown as dots in the first panels to Figs. 2-4 below. The matrix dimension was taken to be $D = 199$, and the complex eigenvalues were chosen to be located on the arc of an ellipse, symmetrically with respect to the real axis.

[7] Every two elements of the Lejá point sequence are different – therefore the denominator in Equ.(18) is always different from zero.

This eigenvalue spectrum resembles a "typical" physical situation insofar as states separated by large frequencies ω_{ij} (corresponding to largely positive or negative imaginary parts of the eigenvalues of $\mathcal{L}$), are connected by "fast dissipation", *i.e.*, also their real parts are large (and negative) [28]. In contrast, eigenvalues closer to the real axis typically have also small real parts [28]. As initial state, a randomly occupied vector $\boldsymbol{\rho}_0$ has been chosen, and propagated for one time step. The shape of the domain G used for interpolation / approximation is taken here as elliptic, and is shown as a solid curve in the first panels of Figs. 2-4. The effects of choosing ellipses G which are different in size and location, can be illustrated with the three exemplary cases of Figs. 2-4. (The results are shown only for the Faber approximation – the Newton expansion behaves similarly.)

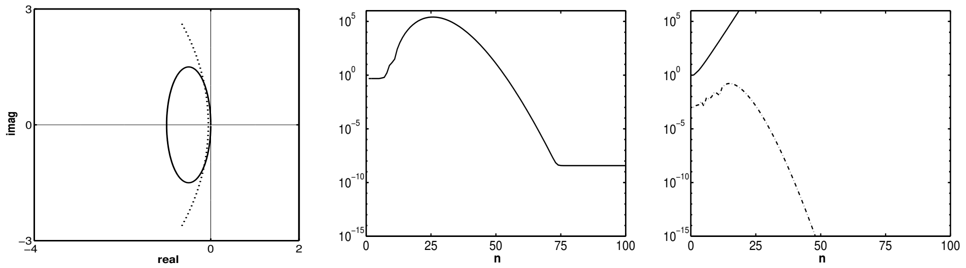

Figure 2: Behaviour of the integration for an *non–scaled* Liouvillian. Starting from the left, the *scaled* domain and the *non–scaled* spectrum ('$\cdots$') are shown in the first graph. The local error (4) versus the order n of approximation is depicted in the center, while in the last picture the Frobenius norm of the Faber polynomials ('—') are presented together with the modulus of the coefficients ('-·-').

In Fig.2, a typical case of numerical instability is presented. It clearly arises from the recursion relation (11) since the so called Frobenius norm

$$||\hat{A}|| := \sqrt{\mathrm{tr}\{\hat{A}^\dagger\ \hat{A}\}}$$

of the last term of the series (13) ($\hat{A} = F_n(\mathcal{L})\hat{\rho}_0$) "explodes", as shown in the third panel of the figure (solid line). This quantity is, therefore, a good measure to control this kind of numerical instability; in contrast, the modulus of the last coefficient c_n is not (dot–dashed curve in the third panel). The recursion relation is unstable because in this case the *non–scaled* eigenvalues of $\boldsymbol{\mathcal{L}}$ lie outside the domain. The local error $\epsilon_{\rm loc}(n)$ [Equ. (4)] grows first exponentially, but then finally decreases to a constant (second panel of Fig. 2). Furthermore, it was shown in [43] that in the above case the remaining error grows exponentially with the time step τ, so for large values of τ the accuracy is completely lost.

Scaling. To avoid these last numerical instabilities in the recursion relation, the Liouvillian has to be scaled:

$$\boldsymbol{\mathcal{L}} \rightarrow \sigma^{-1}\boldsymbol{\mathcal{L}} \quad . \tag{19}$$

The scaling factor $\sigma > 0$ should make the spectrum of $\sigma^{-1}\boldsymbol{\mathcal{L}}$ lie inside the *scaled* domain. As a consequence[8], the step size has to change, too: $\tau \rightarrow \sigma\tau$.

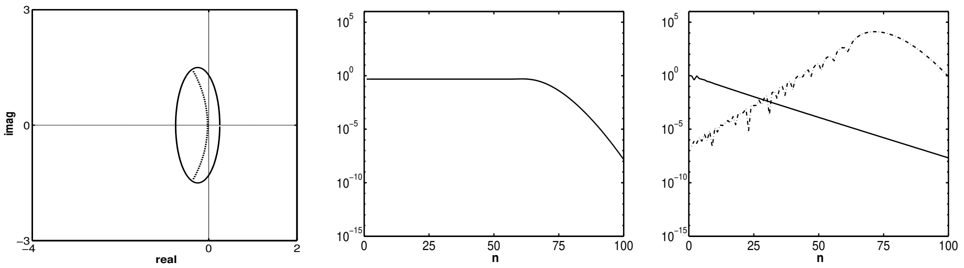

Figure 3: Behaviour of the integration when the Liouvillian is properly scaled but the domain lies partially in the right part of the complex plane. The meaning of the graphs is the same as in Fig. 2.

In Fig. 3, it is shown what happens if the domain is properly scaled but improperly set and enters the right part of the complex plane. This depends on the position of the points for the Newton interpolation and on the parameter m in Equ.(7) for the Faber approximation, respectively. The Frobenius norm of the Faber polynomials decreases exponentially in this case, because the recursion relation is stable. The modulus of the coefficients c_n increases exponentially until $n \approx 70$, where it reaches a value far larger than 1 (which indicates this kind of error), then it starts to decrease. If the center m of the ellipse lies on the imaginary axis, the local error $\epsilon_{loc}(n)$ looks similar to the one shown in Fig. 2. The local error is constant until $n \approx 70$ and then starts to decrease; therefore the calculation finally converges, but the propagation is numerically inefficient because a high polynomial order is required.

In Fig.4, the spectrum of the *scaled* Liouvillian lies entirely in the *scaled* domain, which is completely contained in the left part of the complex plane. The norm of the Faber polynomials is almost constant, showing that the scaling was correct [42]. The modulus of the coefficients is bounded by 1 and decays exponentially from $n \approx 30 = \tau\sigma$ on. The effort to reach a given local tolerance is much less than in the two examples above. The optimal

[8]We have $\boldsymbol{\rho}(\tau) = \exp(\tau\boldsymbol{\mathcal{L}})\boldsymbol{\rho}_0 = \exp(\sigma\tau\ \sigma^{-1}\boldsymbol{\mathcal{L}})\boldsymbol{\rho}_0 \approx P_n^{\sigma\tau}(\sigma^{-1}\boldsymbol{\mathcal{L}})\boldsymbol{\rho}_0$. Note that in general $P_n^{\sigma\tau}(\sigma^{-1}\boldsymbol{\mathcal{L}})\boldsymbol{\rho}_0 \neq P_n^{\tau}(\boldsymbol{\mathcal{L}})\boldsymbol{\rho}_0$, although the identity holds for the exponential function.

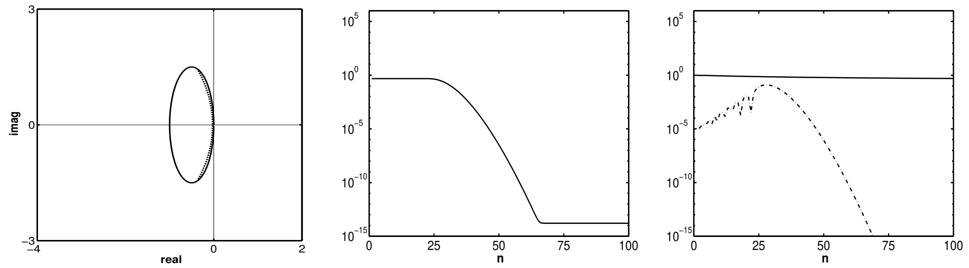

Figure 4: Behaviour of the integration when the Liouvillian is properly scaled and the domain is correctly set. The meaning of the graphs is the same as in Fig. 2.

ellipse has the smallest scaling factor σ compatible with a stable propagation.

In practice, an algorithm is necessary to determine a rough estimate of the region of the complex plane where the eigenvalues of the Liouvillian matrix $\boldsymbol{\mathcal{L}}$ lie. For the Faber algorithm with an ellipitical domain G, this will produce the parameters m (and d) in (7). Also for the Newton algorithm an estimate for the size and shape of the eigenvalue spectrum is required, no matter how G will actually be chosen. In Refs.[28, 29, 30] it was shown how a first guess for the shape and size of the spectrum of $\boldsymbol{\mathcal{L}}$ can be made on the basis of physical arguments (expected maximum Hamiltonian energy difference $|E_i - E_j|$, and fastest dissipative channel).

As a more automatized procedure, in this work we employ the most simple iterative method, the power method [44] to estimate an eigenvalue spectrum. This method is particulaly useful because in the present applications the reasonable assumption can be made that the eigenvalues lie "along the lines" between zero and the eigenvalue of largest modulus – hence only this last one has to be evaluated. To have a reasonably stable iteration, one should consider that:

1. The eigenvalues are distributed symmetrically with respect to the real axis (see above). Accordingly, there are always two eigenvalues with maximum modulus. Adding $iE_{max}\hat{I}$ to the Liouvillian, where E_{max} is an estimate of the maximal energy, the eigenvalue spectrum is translated along the imaginary axis and one of the eigenvalues with maximum modulus becomes larger than the other one.

2. The Frobenius norm and relative scalar product has to be used to

compute the eigenvalue as

$$\lambda = \frac{\mathrm{tr}\{\boldsymbol{\rho}_n^\dagger \boldsymbol{\rho}_{n-1}\}}{\sqrt{\mathrm{tr}\{\boldsymbol{\rho}_{n-1}^\dagger \boldsymbol{\rho}_{n-1}\}}} \quad . \tag{20}$$

3. The iteration procedure has to be repeated a number of times sufficient in order to let the system relax close enough to the desired eigenvalue.

3.2 Spectral estimates, scaling and coefficients

3.2.1 Newton interpolation

In order to stabilize the computation of the Newton polynomials and the divided difference coefficients, the Lejá points have to be scaled [see (15) and (18)]. This is done iteratively: use a few points in the Lejá algorithm to derive a rough estimate of ρ [see (17)] and rescale all points with respect to ρ. Now, use more points to generate a more precise logarithmic capacity, rescale and so on. Repeat this procedure until ρ deviates by less than a prespecified tolerance from 1. Usually no more than three or four iterations are needed.

The generation of the Lejá points requires the repetition of many operations [16]. If we call z_i the i–th point chosen, and $d_n(\tilde{z}_i)$ the product of the distances of point $\tilde{z}_i$ with the n points already chosen, the Lejá algorithm starts as follows:

- The first point z_1 is chosen.
- $d_1(\tilde{z}_i) = \tilde{z}_i - z_1$ for every other point $\tilde{z}_i$ is computed and the $\tilde{z}_i$ with maximal d_1 is chosen as the second point z_2.
- The product $d_2(\tilde{z}_i) = (\tilde{z}_i - z_1)(\tilde{z}_i - z_2) = d_1(\tilde{z}_i)(\tilde{z}_i - z_2)$ is computed, and the maximum value of it determines z_3.
- At every step k the $d_k(\tilde{z}_i) = \prod_{j=1}^{k}(\tilde{z}_i - z_j) = d_{k-1}(\tilde{z}_i)(\tilde{z}_i - z_k)$ is computed and its maximum values determines z_k, until the number of required points, n, is generated.

If the last $d_{k-1}(\tilde{z}_i)$ for all the remaining points in Γ_L is kept in the memory, the algorithm scales as $n(L-n-1)$, where n is the number of points to be chosen for the interpolation and L is the total number of points used by the Lejá algorithm.

3.2.2 Faber approximation

If an eigenvalue λ of maximal modulus is known [see Equ.(20)], it is possible to determine an "optimal" ellipse: Its parameter $m \in [-2, 0]$ solves the third order equation $(1 + r^2)m^3 + (6r^2 - 2)m^2 + 12r^2 m + 8r^2 = 0$ with $r = \mathrm{Im}(\lambda)/\mathrm{Re}(\lambda)$, which can be solved by Newton methods [44, 45]. Since the ellipse should not penetrate the right part of the complex plane, we choose $d = -(m + 1)$. Now, the scaling factor is fixed, too: $\sigma = |\lambda/q|$ for $q = \sqrt{1 + r^2} 2rm(2 + m)^2/(m^2 + r^2(2 + m)^2)$.

The next step is to calculate the coefficients $c_k = \eta_k J_k(2\sigma\tau\sqrt{-d})$ with $\eta_k = (-i/\sqrt{-d})^k \exp(\sigma\tau m)$. Since the density matrix theory in general is applicable in the weak or at least medium coupling limit (for Markovian equations), the spectrum of $\boldsymbol{\mathcal{L}}$ is "near" the imaginary axis and therefore $-1 \leq m \leq 0$. Accordingly, $d \leq 0$ and we need only Bessel functions for purely real arguments. The factor η_k is prone to underflow for large τ and to overflow for large k. For this purpose we calculated η_k in the following way:

$$\eta_k = \left\{ \begin{array}{ll} \{(\frac{-i}{\sqrt{-d}})^{k/\tau} \exp(\sigma m)\}^{\tau}; & |\eta_{k-1}| < 10^{-3}\mathrm{tol} \\ \frac{-i}{\sqrt{-d}}\eta_{k-1} & \mathrm{otherwise} \end{array} \right\}$$

with $\eta_0 = \exp(\sigma m)$ and tol denoting the local tolerance.

3.3 Local error estimator

We have seen in Sec.3.1 that instabilities are detectable by the modulus of the coefficients and the Frobenius norm of the Faber polynomials. Therefore, the term

$$\epsilon_{\mathrm{loc}}(k) \quad = \quad |c_k(\sigma\tau)| \sqrt{\mathrm{tr}\{F_k^* F_k\}}$$

can be used as a local error estimator. The estimator is only valid in the decaying phase, which starts around $n \approx \sigma\tau$ and ends at the constant remaining error level, see Fig.5. Unfortunately, not much about the remaining error level can be said. It is known to grow moderate linearly in τ and D [43], but there seems to be no way of estimation. Since for a stable recursion the Frobenius norm of F_k is usually around 1 the order of the series is taken as high as necessary for the coefficients' modulus to be smaller than the required tolerance. As a stability check one should compute the Frobenius norm of the last Faber polynomial F_n (see above).

Some caution must be taken for the Newton interpolation, since the divided difference coefficients oscillate in the decaying phase. This may cause an underestimation of the real error. To eliminate this problem a simultaneous check on a few coefficients before the last one is usually sufficient.

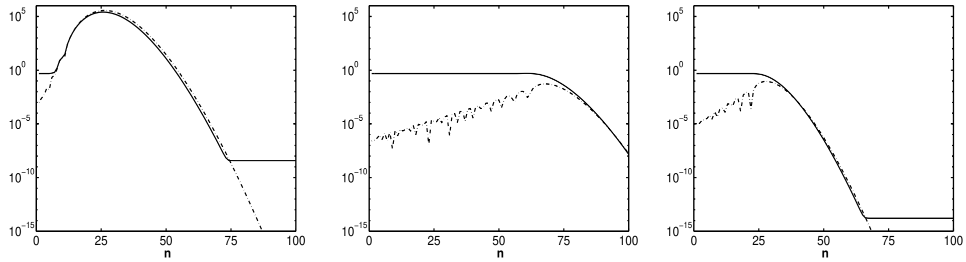

Figure 5: The local error of the Faber approximation ('—') and the Frobenius norm of $c_k(\sigma\tau)F_k(\sigma^{-1}\boldsymbol{\mathcal{L}})\boldsymbol{\rho}$ ('-·-') for the three examples of Figs.2-4. The two curves do behave very similar *in the interesting decaying phase of the local error.*

4 Physical applications

4.1 Damped harmonic oscillator: Comparison between Faber approximation and Newton interpolation

In terms of memory occupation, the two methods are equivalent: The Newton interpolation is based on a two term recursion (15) while the Faber approximation is based on a three term recursion (10). In practice, both need three copies of the matrix $\boldsymbol{\rho}$ to realize the recursive generation of $\boldsymbol{\rho}(t)$, as can be seen from Equs.(11) (Faber) and (16) (Newton), respectively. In both cases the basic operation is $\boldsymbol{\mathcal{L}\rho}$, thus there is no need to store any (super) matrices of size $D \times D = N^2 \times N^2$. The operation $\boldsymbol{\mathcal{L}\rho}$ itself depends on the particular representation used; *e.g.*, in the case of a coordinate grid representation the Hamiltonian operation $\boldsymbol{\mathcal{L}}_H\boldsymbol{\rho}$ is conveniently done *via* a Fast Fourier Transform (FFT) algorithm, which scales as $N^2\log_2 N$ [9].

To test the propagators, a one–dimensional harmonic oscillator coupled to a bath at $T = 0$ K was chosen, following the equation [46]:

$$\dot{\hat{\rho}} = -i\omega[\hat{a}^\dagger\hat{a}, \hat{\rho}] + \gamma\left(\hat{a}\hat{\rho}\hat{a}^\dagger \;-\; \frac{1}{2}[\hat{a}^\dagger\hat{a}, \hat{\rho}]_+\right) \quad , \tag{21}$$

where $[\quad]_+$ denotes an anticommutator, and $\hat{a}^\dagger$ and $\hat{a}$ are the creation and annihilation operators, respectively. ω is the oscillator frequency, and γ a damping constant. Equ.(21) derives from the general form (1) with the identification $\hat{H}_s = \omega(\hat{a}^\dagger\hat{a} + \frac{1}{2})$, and the assumption that the dissipative Liouvillian is of Lindblad form [5]

$$\mathcal{L}_D\hat{\rho} = \sum_i \left(\hat{C}_i\hat{\rho}\hat{C}_i^\dagger - \frac{1}{2}\left[\hat{C}_i^\dagger\hat{C}_i, \hat{\rho}\right]_+\right) \tag{22}$$

Table 1: Damped harmonic oscillator: Typical polynomial order necessary for a Newton and a Faber polynomial series to achieve a relative error in the energy smaller than 10^{-4}. "n.s." means not stable.

time step τ [a.t.u.]	100	400	1000	2000	3000
Faber	277	1059	2509	5249	7795
Newton	273	1067	2545	5662	n.s.

(i labels different dissipative channels). In the damped oscillator case (21), we use a single Lindblad operator $\hat{C}$, which is $\hat{C} = \sqrt{\gamma}\hat{a}$.

By choosing $\omega = 0.02$ E_h and $\gamma \approx 10^{-2}\omega$, weak damping was anticipated. Further, the system was represented on a spatial grid of 128 points, although a harmonic oscillator basis should do equally well. As initial state, we assume that the oscillator is at $t = 0$ in its first excited state, *i.e.*, $\hat{\rho}_0 = |\psi_1\rangle\langle\psi_1|$, where $|\psi_1\rangle$ is the first excited harmonic oscillator function.

In Table 1, we compare the performance of the Newton–Lejá and Faber algorithms by propagating one time step τ and determining the corresponding polynomial order n which is required to keep the relative error in the energy smaller than 10^{-4}. From the table we note that the two algorithms behave quite similar, *i.e.*, about the same polynomial order (and hence computation time) is required to achieve the same accuracy, with small advantages for the Faber algorithm. Hence, both algorithms are similar not only in their mathematical structure, but also in their numerical efficiency. This was confirmed in a series of test calculations with varying parameters ω and γ.

The advantages of the Faber algorithm are that (i) it is stable to higher orders than the Newton algorithm (see Table 1), (ii) the coding of a computer program is definitely easier, and (iii) no selection of sampling points has to be made. On the other hand, for the Newton interpolation, there are no restrictions on the analytic function to be applied to; also; there is no restriction on the shape of the domain G chosen to enclose the complex eigenvalue spectrum of the Liouvillian, whereas the Faber approach requires a different implementation if domains different from the elliptical one are adopted. It should be noted, however, that the choice of an optimal enclosing domain is difficult in general, simply because the eigenvalue spectrum is not known. Therefore, working with a fixed domain shape (*e.g.*, an elliptical one) is only a moderate disadvantage in practice.

4.2 Absorption spectra by polynomial expansions

4.2.1 Polynomial expansion of an absorption spectrum

Often, the propagated density matrix is used in other formulae to derive observables of interest. A typical case is the computation of a continuous wave (cw) absorption spectrum. For a weak, continuous wave field, there is a known expression for the absorption coefficient of a system embedded in a dissipative environment [47]

$$\alpha(\omega) = \frac{4\pi\omega n_{mol}}{nc} \,\mathrm{Re} \int_0^\infty dt\; e^{i\omega t}\, \mathrm{tr}\left\{\hat{\mu} e^{\mathcal{L}t} \left[\hat{\mu}, \hat{\rho}_0\right]\right\} \quad , \tag{23}$$

which can be viewed as a generalization of the so called Heller formula [48] to the dissipative case. Here ω is the light frequency, $\hat{\mu}$ is the dipole operator, n_{mol} is the density of molecules, c the velocity of light, and $\hat{\rho}_0$ the initial density operator. Setting $\hat{\rho}_0' := [\hat{\mu}, \hat{\rho}_0]$, the solution of (23) is equivalent to the propagation of a matrix according to the dissipative LvN equation (1). The integration is done for a discrete number of time steps, the trace is computed for each time step and Fourier transformed.

An interesting aspect of the polynomial integrators is that the time dependence is only in the coefficients and the representation dependence is left in the Faber or Newton recursion relations [1, 31, 49]. In the case of the Faber approximation, for example,

$$e^{\mathcal{L}t} \left[\hat{\mu}, \hat{\rho}_0\right] \approx \sum_{k=0}^{n} c_k(t) F_k(\mathcal{L}) \hat{\rho}_0' \quad . \tag{24}$$

This implies that (23) in its polynomial approximation (24) can be rewritten as

$$\alpha(\omega) \approx K_s \mathrm{Re} \sum_{k=0}^{n} \underbrace{\omega \int_0^\infty e^{i\omega t} c_k(t) dt}_{s_k(\omega)} \;\mathrm{tr}\{\hat{\mu} F_k(\mathcal{L}) \hat{\rho}_0'\}, \tag{25}$$

where $K_s := \frac{4\pi n_{mol}}{nc}$ and the only approximation is in the polynomial expansion of the propagator, and where the trace is time–independent. In contrast to the Newton expansion, the Faber coefficients $c_k(t)$ are given analytically by Equ.(14). Using (14), also the coefficients $s_k(\omega)$ of the Faber approximation for spectrum evaluation in (25) can be evaluated analytically as [50]:

$$
\begin{aligned}
s_k(\omega) &= \omega \int_0^\infty e^{i\omega t} c_k(t) dt \\
&= \omega \left(\frac{-i}{\sqrt{-d}} \right)^k \int_0^\infty e^{i\omega t} e^{m\sigma t} J_k(2\sigma t \sqrt{-d}) dt \\
&= \frac{\omega}{\sqrt{4\sigma^2 d + (m\sigma + i\omega)^2}} \left(\frac{\sqrt{4\sigma^2 d + (m\sigma + i\omega)^2} + (m\sigma + i\omega)}{2\sigma d i} \right)^k
\end{aligned} \quad (26)
$$

These coefficients are very similar to the Chebychev series for computing dissociative Raman spectra [1] or the Faber series for the Green operator [31]. This is to be expected because the underlying framework of the three series is equivalent.

Hence, the evaluation of absorption spectra for condensed phase problems can be done semi-analytically by using (25), with the coeffcients given by (26). Unlike the Faber coefficients $c_k(t)$, the coefficients $c_k(\omega)$ (26) for spectra evaluation are algebraic and therefore no special functions like Bessel functions are needed. This makes the series very stable and polynomial orders up to millions can be used without problems. However, a different series is needed for every frequency ω. For a given ω, the terms in (26) are generated via a simple one term recursion relation – the $(k+1)$st coefficient is readily calculated from the k th one.

4.2.2 Infrared absorption spectrum of benzoic acid dimers

The new series was applied to the IR absorption spectrum of benzoic acid dimers embedded in benzoic acid crystals. For this pourpose, a two–dimensional model of the double minimum type was used, which is described elsewhere [51, 52]. The model consists of a "hydrogen transfer mode" and a "molecular frame mode", and all operators were represented in the basis of the (16 lowest) vibrational bound states of the model Hamiltonian $\hat{H}_s$. The system vibrational levels $|i\rangle$ relax due to vibrational energy dissipation, caused by the coupling to the phonons of the embedding crystal. The relaxation was taken to be of the Lindblad form (22), with

$$
\hat{C}_i \rightarrow \hat{C}_{kl} = \sqrt{\Gamma_{kl}} |k\rangle\langle l| \quad ,
$$

where the Γ_{kl} are relaxation rates connecting two vibrational states. For the evaluation of Γ_{kl}, a microscopic model was used. All details of the model and the parameters are from Refs. [52] and [51].

In Ref. [52], the spectrum was obtained by numerically propagating a matrix $\boldsymbol{\rho}'_0$ [Equ. (23)] with a Newton polynomial integrator. Here we use the semi–analytic series (25). When the dissipation is of simple Lindblad form, there is also an analytical solution for $\alpha(\omega)$ [47, 52]. The analytical spectrum is then a sum of broadened Lorentzians [52]:

$$\begin{aligned}\alpha(\omega) &= \omega \sum_{i>j} {\mu_{ij}}^2 \, (g_j - g_i) \\ &\left(\frac{\Gamma_{ii}+\Gamma_{jj}}{(\Gamma_{ii}+\Gamma_{jj})^2 + (\omega+\omega_{ji})^2} - \frac{\Gamma_{ii}+\Gamma_{jj}}{(\Gamma_{ii}+\Gamma_{jj})^2 + (\omega-\omega_{ji})^2} \right) \end{aligned} \tag{27}$$

Here, the μ_{ij} are the matrix elements of the dipole moment operator, ω_{ij} is the frequency for transitions between levels $|i\rangle$ and $|j\rangle$, and g_i is the Boltzmann weight for state $|i\rangle$ at temperature T, *i.e.*, $g_i = e^{-\frac{E_i}{k_b T}}/Q$ (k_b the Boltzmann constant, E_i the energy of state $|i\rangle$, and $Q = \sum_{i=0}^{\infty} e^{-\frac{E_i}{k_b T}}$ the partition function). For the diagonal elements of the relaxation matrix we used the definition $\Gamma_{ii} = \sum_{j \neq i} \Gamma_{ji}$, as in Ref.[52].

Before considering the spectrum itself, we comment on the behaviour of the expansion coefficients $s_k(\omega)$ as a function of ω and the strength of dissipation (*i.e.*, temperature). From Fig.6, where $s_k(\omega)$ is shown as a function of ω, it is clear that the smallest ω can be taken as a reference for the convergence of all series, *i.e.*, the low–ω part of the spectrum requires the highest polynomial order to converge a spectrum, while at higher ω the computational effort becomes smaller.

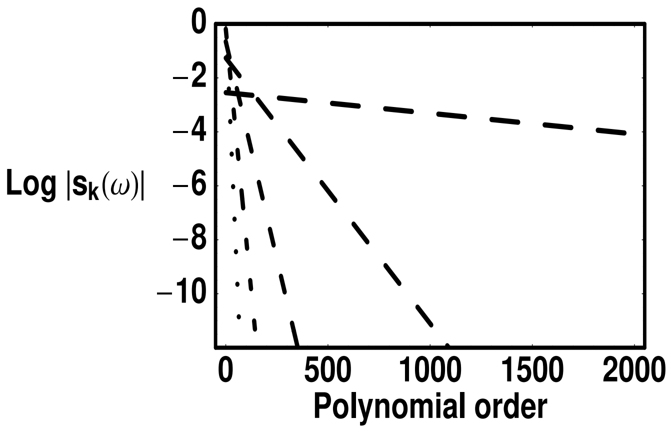

Figure 6: Computation of spectra by polynomial expansion. The logarithm of the coefficient $|s_k(\omega)|$ as a function of the polynomial order is plotted for $\omega = 0.2$, 0.7, 1.2, 1.7, 2.2 E$_h$; m is set to 0.2 E$_h$ and $\sigma = 1.2$. The bigger ω, the smaller are the dashes of the dashed lines.

In Fig.7 effects of the dissipative strength are considered, which can be investigated by varying the parameter m in Equ.(7). One finds that for stronger dissipation (larger modulus of m), the modulus $|s_k(\omega)|$ of the expansion coefficients decay more rapidly with k than in weakly dissipative cases. This means that the series (25) converges faster when the dissipation is strong, and the computation of spectra is less costly in this case. Strong dissipation is characterized by large Lorentzian line widths according to Equ.(27). In contrast, when dissipation is weak and the peaks are narrow (*e.g.*, at low temperature), larger polynomial orders are required. Further, in order to resolve narrow peaks many points ω_i are needed at which $\alpha(\omega_i)$ has to be calculated.

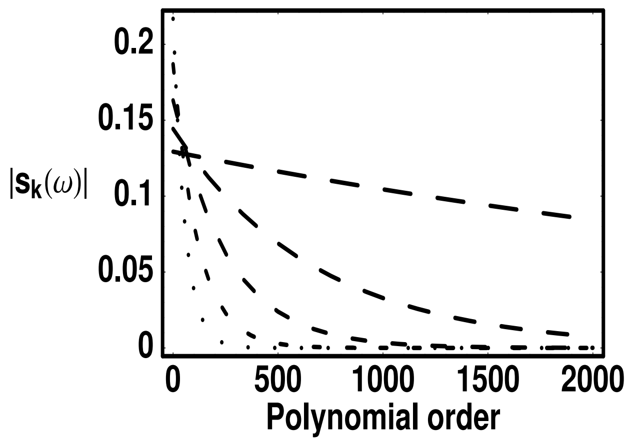

Figure 7: Computation of spectra by polynomial expansion. The modulus of the coefficients $|s_k(\omega)|$ is plotted as a function of the polynomial order for $m = -.05, -.25, -.45, -.65, -.85$ E$_h$; ω is set to 0.2 E$_h$ and $\sigma = 0.8$. The bigger the modulus of m the smaller are the dashes in the dashed lines .

In Fig.8 we show the IR absorption spectrum of the benzoic acid dimer in a crystal as obtained with our two–mode model [51, 52] according to Equ.(25) for various crystal temperatures T. The well known trends are observed, that (1) temperature increases the magnitude of dissipation and hence makes the peaks broader, and (2) higher temperatures favour the contribution of "hot bands" to the high–ω part of the spectrum. All spectra obtained *via* (25) are in complete agreement with the analytical solution (27) (when the antiresonant terms are included), and it is not possible to distinguish between the analytical and the semi-analytical curves on the scale of Fig.8. There is a certain quantitative disagreement with the spectra reported in Ref. [52], thus showing that the present approach can improve accuracy in computing spectra in the presence of dissipation.

We do not analyze and assign the spectrum in detail here – that has

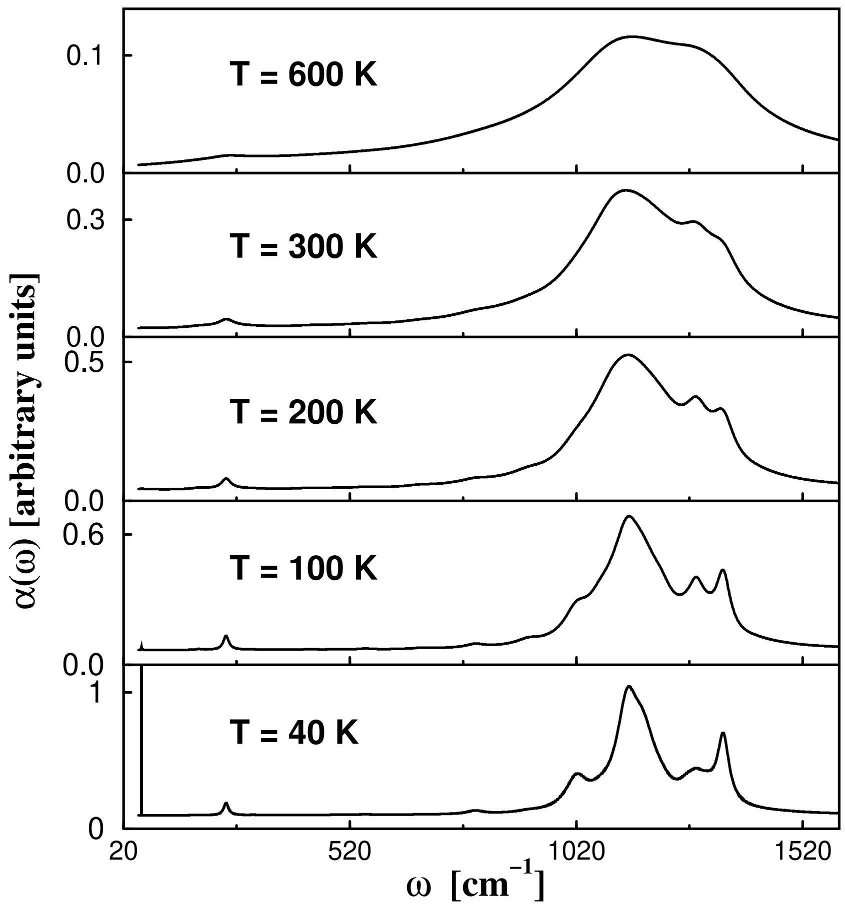

Figure 8: Benzoic acid dimer, embedded in a crystal. IR absorption spectra computed for $T = 40, 100, 200, 300$K (from lowest to highest frame). The spectra are scaled in order to keep the peak at ≈ 1140 cm^{-1} at 80 % of the height of the frame. For the lowest temperature a very high peak emerges at 59.76 cm^{-1}, whose features are plotted in Fig. 9, at the same vertical scale. The analytical spectra are indistinguishable from the computed ones.

already been done elsewhere [52]. It is enough to note that the different (broadened) lines correspond to either (double–) hydrogen transfer or molecular frame modes. From Fig.8 we note that in particular at very low temperatures (*e.g.*, at $T = 40$ K), there exists a very sharp peak right below $\omega = 60$ cm^{-1}, which corresponds to the hydrogen transfer mode. This peak is particularly hard to compute by a series expansion, because (i) ω is small (which is unfavourable according to Fig.6), (ii) the dissipation is weak (which is unfavourable according to Fig.7, and because many ω_i are needed).

To converge the 40K spectrum around $\omega = 60$ cm^{-1}, a series of order $n = 4 \cdot 10^7$ was needed, which took about 40 min of CPU time on a medium–sized workstation. For this calculation, the ratio between the modulus of the last coefficient and the first one, $c_n(\omega)/c_0(\omega)$, was set to 10^{-7}. Fig.9, which is a blow–up of the spectrum around the 60 cm^{-1} peak, shows that this accuracy is indeed sufficient to give agreement with the analytical result even on a high–resolution scale. Also, with a ratio $c_n(\omega)/c_0(\omega) = 10^{-5}$ the series (25) gives a reasonable agreement with the analytical answer. However, by choosing $c_n(\omega)/c_0(\omega) = 10^{-3}$, the semi–analytical peak becomes too broad, and artificial oscillations emerge at the wings of the Lorentzian.

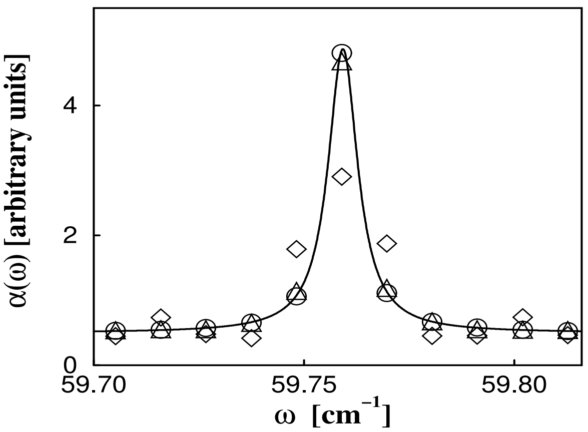

Figure 9: The absorption spectrum around the peak at 59.76 cm^{-1} is shown as computed for three different ratios $c_n(\omega)/c_0(\omega)$ of the moduli of the last and first expansion coefficients: 10^{-7} (circles), 10^{-5} (triangles) and 10^{-3} (diamonds). The analytical solution is depicted as a solid line.

In contrast for other peaks of the spectrum a ratio of 10^{-3} gives a spectrum almost indistinguishable from the analytical one, even at temperatures as low as $T = 40$K. At the same time, for larger ω a shorter polynomial expansion suffices to make the ratio $c_n(\omega)/c_0(\omega)$ small (see Fig.6). At $\omega \approx 1200$ cm^{-1}, for example, we require only $n \approx 2 \cdot 10^3$ terms to converge the spectrum with $c_n(\omega)/c_0(\omega) = 10^{-3}$. And even $c_n(\omega)/c_0(\omega) = 10^{-7}$ requires only $n \approx 8 \cdot 10^3$ in this case.

4.3 More general applications

The application of Newton or Faber polynomial integrators is neither restricted to Lindblad dissipation (22), nor to time–independent Liouvillians. For illustration, we considered a double minimum potential hydrogen transfer model similar to the one described in the last subsection (see Ref.[53])

for details), with two important differences: (1) The hydrogen transfer was driven by coupling the molecular dipole to an explicitly time–dependent, pulsed electromagnetic field in the IR frequency domain, and (2) the dissipation was of Redfield form, *i.e.*, elementwise,

$$(\mathcal{L}_D \hat{\rho})_{kl} = \sum_{i,j} R_{kl,ij} \ \rho_{ij} \quad . \tag{28}$$

Here, the elements of the relaxation tensor, $R_{kl,ij}$, and all other computational parameters where taken from Ref.[53]. In contrast to Lindblad dissipation, Equ.(28) allows for the coupling of diagonal and off–diagonal density matrix elements, as well as for the coupling between different off–diagonal elements.

For these applications, it turned out that even in the case of a rapidly oscillating driving field, both the Newton–Lejá and the Faber expansion can outperform a standard Runge–Kutta integrator in terms of computation time. This was particularly so when when high accuracy was demanded for. This is not necessarily to be expected, since polynomial expansions are (due to their exponential convergence [1]), most efficient when large polynomial orders and large timesteps can be used.

It further appears that the polynomial integrators are general enough to cope not only with Lindblad forms of dissipation, in contrast, *e.g.*, to stochastic wave packet methods [18]. Even when the dissipation is chosen artificially strong, in which case the Redfield form (28) leads to physically meaningless negative eigenvalues of the density matrix, the polynomial integrators proved to be stable – only special care had to be taken during the scaling procedure.

5 Conclusions

In conclusion, both the Newton–Lejá interpolation and the Faber approximation are very valuable tools to integrate a Markovian, open–system Liouville–von Neumann equation (1) in time. Both integrators are stable and accurate; various measures can be given to keep their accuracy well under control. In particular the Faber approximation appears to be highly stable and easy to implement; it further leads to an efficient, semi–analytical series expansion for the linear absorption coefficient for condensed phase spectra. Both algorithms are found to be fast (even for explcitly time–dependent problems), and general (the dissipative Liouvillian must only be Markovian).

These propagators will therefore be useful not only when a benchmark solution is required, but also for physical applications where other methods cannot easily be used in practice. Also, the polynomial expansion of others than the exponential function of a Liouvillian will be of interest. Finally, a critical comparison of the polynomial integrators presented here to *e.g.* the split–operator integrators [8, 10, 27] should be a rewarding task for the future.

ACKNOWLEDGMENTS

Fruitful discussions with Ch. Schütte (Konrad-Zuse-Zentrum, Berlin) are gratefully acknowledged. We thank N. Doslic (Free University Berlin) for providing a density matrix code with Redfield dissipation. We thank the Deutsche Forschungsgemeinschaft (DFG) (project no. Sa 547/2-2) for supporting this project.

References

[1] See, for example: R. Kosloff, Annu. Rev. Phys. Chem. 45, 145 (1994), and references therein.

[2] K. Blum, *Density matrix theory and applications* (Plenum, New York, 1981).

[3] D. Kohen, C.C. Marston, and D. J. Tannor, J. Chem. Phys. **107**, 5141 (1997).

[4] A.G. Redfield, Advan. Magn. Reson. **48**, 119 (1956).

[5] G. Lindblad, Commun. Math. Phys. **48**, 119 (1976).

[6] V. Gorini, A. Kossakowski, and E.C.G. Sudarshan, J. Math. Phys. **17**, 821 (1976).

[7] A.O. Caldeira and A. Legget, Physica A **121**, 587 (1983); I. Oppenheim and V. Romero-Rochin, Physica A **147**, 184 (1987); Y.J. Yan and S. Mukamel, J. Chem. Phys. **88**, 5735 (1988); A. Suárez, R. Silbey, and I. Oppenheim, J. Chem. Phys. **97**, 5101 (1992); A.M. Walch and R.D. Coalson, Chem. Phys. Lett. **198**, 293 (1992);

[8] B. Hellsing and H. Metiu, Chem. Phys. Lett. **127**, 45 (1986).

[9] M. Berman and R. Kosloff, Comp. Phys. Commun. **63**, 1 (1991).

[10] W.K. Lai, K.-A. Suominen, B.M. Garraway, and S. Stenholm, Phys. Rev. A **47**, 4779 (1993).

[11] V. May, O. Kühn, and M. Schreiber, J. Phys. Chem. **97**, 12591 (1993).

[12] W.T.Pollard and R.A.Friesner, J. Chem. Phys. **100**, 5054 (1994).

[13] B. Jackson, J. Chem. Phys. **108**, 1131 (1997).

[14] L. Pesce and P. Saalfrank, Chem. Phys. **219**, 43 (1997).

[15] L. Pesce and P. Saalfrank, J. Chem. Phys. **108**, 3045 (1998).

[16] G. Ashkenazi, R. Kosloff, S. Ruhmann, and H. Tal-Ezer, J. Chem. Phys. **25**, 1283 (1992).

[17] R. Dum, P. Zoller, and H. Ritsch, Phys. Rev. **A 45**, 4879 (1992).

[18] K. Mølmer, Y. Castin, and J. Dalibard, J. Opt. Soc. Am. **B10**, 524 (1993).

[19] H.-P. Breuer and F. Petruccione, Phys. Rev. E **52**, 428 (1995).

[20] B. Wolfseder and W. Domcke, Chem. Phys. Lett. **235**, 371 (1995).

[21] P. Saalfrank, Chem. Phys. **211**, 265 (1996).

[22] N. Gisin and I.C. Percival, J. Phys. A **25**, 5677 (1992).

[23] B.M. Garraway and P.L. Knight, Phys. Rev. A **49**, 1266 (1994).

[24] T. Gerdts and U. Manthe, J. Chem. Phys. **106**, 3017 (1996).

[25] L. Pesce, T. Gerdts, U. Manthe, and P. Saalfrank, Chem. Phys. Lett. **390**, 288 (1998).

[26] J.M. Jean, R.A. Friesner, and G.R. Fleming, Chem. Phys. **96**, 5827 (1992).

[27] I. Burghardt, J. Phys. Chem. A **102**, 4192 (1998).

[28] M. Berman, R. Kosloff, and H. Tal-Ezer, J. Phys. A: Math. Gen. **25**, 1283 (1992).

[29] A. Bartana, R. Kosloff, and D. Tannor, J. Chem. Phys. **99**, 196 (1993); U. Banin, A. Bartana, S. Ruhman, and R. Kosloff, J. Chem. Phys. **101**, 8461 (1994).

[30] P. Saalfrank, R. Baer, and P. Saalfrank, Chem. Phys. Lett. **230**, 463 (1994); P. Saalfrank and R. Kosloff, J. Chem. Phys. **105**, 2441 (1996)

[31] Y. Huang, D.J. Kouri, and D.K. Hoffmann, Chem. Phys. Lett. **225**, 37 (1994); Y. Huang, D.J. Kouri, and D.K. Hoffmann, J. Chem. Phys. **101**, 10493 (1994).

[32] J.B. Conway, *A Course in Functional Analysis* (Springer, Berlin, 1990).

[33] S. Lang, *Complex Analysis*, (Springer, Berlin, 1993).

[34] S. W. Ellacott, Mathematics of Computation **40**, 575 (1983); S. W. Ellacott, Comput. Math. Appl. **12B**, 1103 (1986).

[35] L. N. Trefethen, J. Approx. Theory **31**, 344 (1981).

[36] L. Reichel, BIT **30**, 332 (1990).

[37] D. Gaier, *Vorlesungen über Approximation im Komplexen* (Birkhäuser, 1980).

[38] P. Henrici, *Applied and Computational Complex Analysis*, volume 3 (John Wiley and Sons, New York, 1986).

[39] W. Huisinga, *Diploma thesis* (Freie Universität Berlin, 1997), available via http://www.zib.de/huisinga.

[40] V. I. Smirnov and N. A. Lebedev, *Functions of a Complex Variable, Constructive Theory* (M. I. T. Press, 1986).

[41] I. N. Bronstein and K. A. Semendjajew, *Taschenbuch der Mathematik* (Verlag Harri Deutsch, Thun, 1989).

[42] H. Tal-Ezer, Contractor Report 87-63, NASA (1987); H. Tal-Ezer, Contractor Report 88-39, NASA (1988).

[43] P. Nettesheim, W. Huisinga, and C. Schütte, Preprint SC-96-47, Konrad-Zuse-Zentrum für Informationstechnik Berlin (1996).

[44] E. Kreyszig, *Advanced Engineering Mathematics* (John Wiley & Sons, New York, 7th ed., 1993).

[45] P. Deuflhard and A. Hohmann, *Numerical Analysis. A First Course in Scientific Computation* (de Gruyter, Berlin, 1995).

[46] R. Alicki and K. Lendi, *Quantum Dynamical Semigroups and Applications*, volume 286 of *Lecture Notes in Physics* (Springer, Berlin, 1987).

[47] F. Neugebauer, D. Malzahn, and V. May, Chem. Phys. **201**, 151 (1995).

[48] E. J. Heller, J. Chem. Phys. **62**, 1544 (1975).

[49] H. Guo, Chem. Phys. Lett. **289**, 396 (1998).

[50] I.S. Gradshteyn and I.M. Ryzhik, *Tables of Integrals, Series, and Products* (Academic, New York, 1980).

[51] R. Meyer and R. R. Ernst, J. Chem. Phys. **93**, 5518 (1990).

[52] Ch. Scheurer and P. Saalfrank, J. Chem. Phys. **104**, 2869 (1996).

[53] N. Došlić, O. Kühn, and J. Manz, Ber. Bunsenges. Phys. Chem. **102**, 292 (1998).